Pergamon

Int. J. Heat Mass Transfer. Vol. 39, No. 12, pp. 2449–2461, 1996

0017-9310/96 $15.00 + 0.00

0017-9310(95)00343-6

Hemispherical vapor bubble growth in microgravity: experiments and model

HO SUNG LEE and HERMAN MERTE, JR†

The University of Michigan, Department of Mechanical Engineering and Applied Mechanics, Ann Arbor, MI 48109-2125, U.S.A.

(*Received* 30 *March* 1995 *and in final form* 12 *September* 1995)

Abstract—Measurements of vapor bubble growth were made in microgravity using R-113 with transient heating at a flat surface, and comparisons made with a combination of two one-dimensional spherical models; an initially uniform superheat model, using the highest temperature at nucleation, denoted as the upper bound of growth, while the second model uses the non-uniform temperature distribution at nucleation as the initial condition surrounding the critical size vapor bubble, denoted as the lower bound. A bubble growth fraction is introduced, related to the upper and lower bounds, and provides a simple index to describe the vapor bubble growth. Copyright © 1996 Elsevier Science Ltd.

1. INTRODUCTION

The understanding of vapor bubble growth on a heater surface in microgravity or the absence of buoyancy is an important step toward describing the associated heat transfer, not only in microgravity but perhaps also in earth or higher gravity levels. A transient heating process in microgravity can provide, at the minimum, known temperature distributions at nucleation and subsequent bubble growth, under a variety of circumstances not otherwise possible in normal gravity fields for purposes of testing this understanding. Measurements of vapor bubble growth and collapse in earth gravity are generally quite non-reproducible because of the randomness of the temperature distribution in the vicinity of the growing vapor bubble, resulting from the turbulence associated with the natural and/or forced convection present, and from the liquid agitation produced by adjacent or prior bubbles. The randomness can be eliminated by instituting a transient heating process of a stagnant liquid to the onset of boiling under microgravity conditions.

Previous experiments involving boiling in reduced gravity have been conducted and reported by Usiskin and Siegel [1], Merte and Clark [2], Littles and Walls [3], Ervin *et al.* [4], Straub *et al.* [5], Merte *et al.* [6] and Abe *et al.* [7], using various facilities; parabolic aircraft flights, sounding rockets, and free fall in drop towers. Little attention has been devoted to the details of vapor bubble growth on the heater surface because of the relatively short periods of time available, with the major emphasis being rather on the heat transfer itself.

Transient pool boiling experiments were conducted on three space flights (STS-47, -57, -60) as part of a NASA Get Away Special (GAS) program in September 1992, June 1993 and February 1994, respectively, with each flight experiment consisting of nine test runs of duration up to 120 s. Measurements of early vapor bubble growths on a relatively large flat heating surface were obtained in which the initial conditions are quite well defined as a consequence of the absence of buoyancy. The results of some of these measurements are presented here for those cases where the early bubbles were observed to be approximately spherical, together with an analytical characterization of this spherical vapor bubble growth in an initially non-uniform one-dimensional Cartesian temperature distribution.

Vapor bubble dynamics in non-uniform temperature fields find extensive applications in diverse areas of pool and forced convection boiling, including cavitation, ultrasonic cleaning, bubble jet printers, and acoustics. The number of analytical works related to such vapor bubble growth on a flat heater surface is relatively small because of the complexity introduced by the combination of flat and curved interfaces with non-uniform temperatures.

Han and Griffith [8] derived a closed-form expression for bubble growth with quasi steady pool boiling in earth gravity, considering one-dimensional heat conduction surrounding the bubble, with the bubble beginning to grow from an arbitrary-sized cavity. Mikic *et al.* [9] predicted the bubble growth in a non-uniform temperature field by correcting an initial uniform superheat model, considering only heat diffusion. In both of these works it was assumed that the liquid at a uniform temperature comes into contact with the heater surface at a given temperature, and after a waiting time the vapor bubble forms and grows in the non-uniform temperature field resulting during

† Author to whom correspondence should be addressed.

NOMENCLATURE

α	thermal diffusivity	t^*	delay time between onset of heating and nucleation
F_{BG}	bubble growth fraction	T	temperature
k_l	thermal conductivity of liquid	T_0	initial bulk temperature
P_{sys}	system pressure	T_w^*	mean heater surface temperature at nucleation
q_l''	heat flux to the liquid	ΔT_{sup}	local heater surface superheat at nucleation
q_T''	total heat flux applied	ΔT_{sub}	bulk liquid subcooling.
r	radial coordinate		
t	time		

this waiting time, followed by departure due to buoyancy.

The present experiments and the prior ones of Ervin *et al.* [4] disclosed two categories of bubble growth: one with bubbles having a smooth surface and what is termed moderate growth rates; the other with bubbles having what appears to be a roughened interface, accompanied by extremely large growth rates, sometimes classified as violent. The work here focuses on the dynamics of those growing vapor bubbles having a smooth surface, and beginning from surrounding non-uniform initial temperatures.

To understand the mechanisms associated with the vapor bubble dynamics more fully, a one-dimensional spherical model was formulated simultaneously incorporating momentum, energy, surface tension and viscosity. The treatment for an initially uniformly superheated bulk liquid is presented in Lee and Merte [10]. This model can also be used to predict vapor bubble growth and collapse arising from initially non-uniform temperature fields following nucleation. The results of some computations will be presented below. However, vapor bubble growth from plane heater surfaces can not be accommodated, since the dynamics of this geometry inherently involve 2D or 3D considerations. An example of interferometric temperature measurements by Straub *et al.* [11] is given in Fig. 1 for such a configuration. As will be demonstrated, the combination of the initially uniform and non-uniform superheated liquid models provide upper and lower bounds for predicting the vapor bubble growth and collapse dynamic processes. The alternative is to solve the 3D case simultaneously incorporating momentum, energy, surface tension and viscosity, with the 3D interface shape becoming a part of the solution process. Computational possibilities for such are not yet available. Computations with the present model, on the other hand, provide reasonable approximations to observed behaviors.

2. EXPERIMENTAL APPARATUS AND PROCEDURE

Bubble growth measurements with R-113 were conducted in the microgravity of space, providing on the order of a/g approx 10^{-4}, as one component of pool boiling experiments. A total of nine tests were conducted, each lasting up to two minutes, at three levels of heat flux and three levels of subcooling, in each of three space experiments. Photographs of the boiling process were obtained simultaneously from the side and from beneath the heater surface at framing rates of 10 and 100 fps.

Figure 2 presents a schematic diagram of the test vessel, consisting of R-113 and nitrogen (N_2) chambers. The R-113 chamber has internal dimensions of 15.2 cm i.d. $\times$ 10.2 cm high, and includes a gold film heater on a quartz substrate, a pressure transducer, thermistors, and stirrer. The stirrer functions to provide a timely uniform fluid temperature between each test. The pressure transducer measures the system pressure with an uncertainty of ± 0.345 kPa, while thermistors measure the liquid temperatures adjacent to the heater surface at distances of 1, 5, 10 mm, and at various other locations, with a total uncertainty of ± 0.06°C. The nitrogen chamber is used to maintain the desired system pressure. System subcooling was obtained by increasing the system pressure above the saturation pressure corresponding to the initial liquid temperature. In the absence of buoyancy, an initially motionless liquid remains stagnant upon heating until the onset of boiling, and the temperature distribution at the moment of incipient boiling can be determined from a conduction heat transfer analysis.

Two heater surfaces are placed on a single flat substrate, installed so as to form one wall of the test vessel as shown in Fig. 2, with one acting as a back-up. Each heater consists of a 400 Å thick semi-transparent gold film sputtered on a highly polished quartz substrate, seen in Fig. 3, and serves simultaneously as a heater, with an uncertainty of $\pm 2\%$ in the measurement of the heat flux, and a resistance thermometer, with an overall uncertainty of ± 1.0°C. The heater is rectangular in shape, 19.05 $\times$ 38.1 mm (0.75 $\times$ 1.5 inch). Degassed commercial grade R-113 (trichlorotrifluorethane, CCl_2FCClF_2) was used because of its low normal boiling point (47.6°C), which minimized problems associated with heat loss to the surroundings, and because of its electrical nonconductivity, which is compatible for direct contact with

Fig. 1. Temperature field around a downward facing R-113 vapor bubble by means of holographic interferometery (Straub *et al.* [11]).

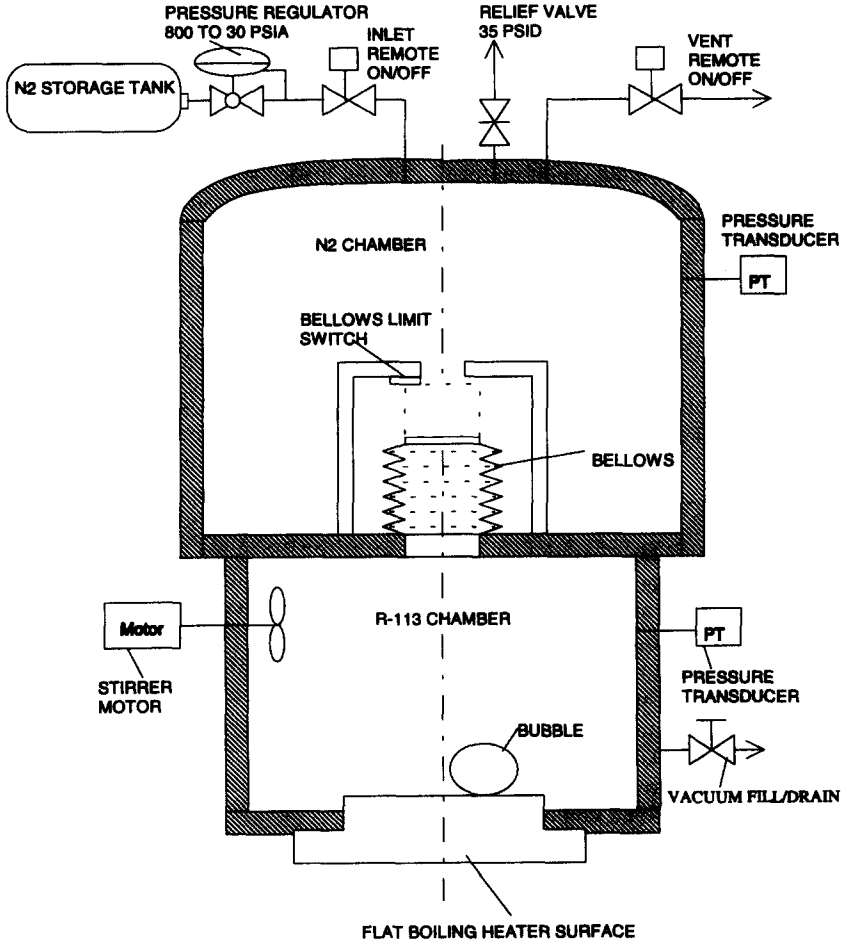

Fig. 2. Schematic of test vessel with concept to provide constant pressure and initially uniform fluid temperature.

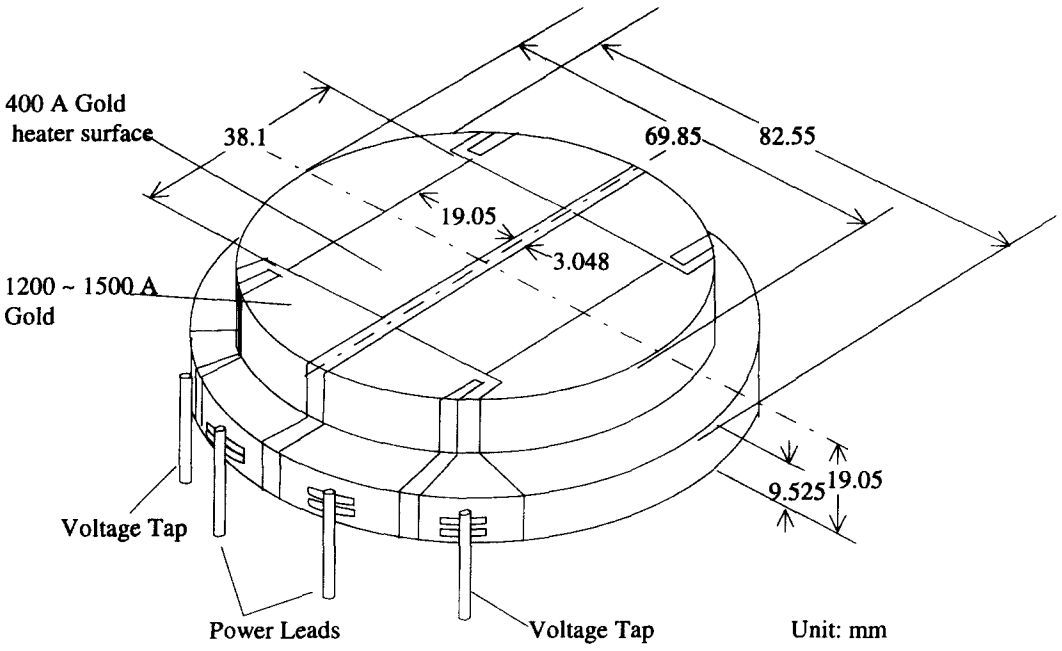

Fig. 3. Transparent gold film heater/resistance thermometer on quartz substrate.

the thin gold film heater. Further experimental details may be found in Merte *et al.* [12].

After a uniform temperature in the quiescent liquid is achieved, the desired heat flux is applied to the heater surface so that a temperature distribution adjacent to the heater surface is produced by transient conduction. After a certain delay time, a non-uniform superheat is reached sufficient to cause nucleation and subsequent vapor bubble growth. The shape of the bubble remains spherical or hemispherical during the very early stages of growth, to be demonstrated photographically, but then becomes deformed as spreading across the heater surface takes place. Once deformation takes place measurements of bubble growth for present purposes is halted, since only smooth spherical bubbles are considered here.

3. MODELING

A realistic thermal boundary layer around an early hemispheric vapor bubble, arising with transient heating from a flat heater surface, is shown schematically in Fig. 4(a), to be compared with the measurement in Fig. 1. An attempt is made here to describe the bubble growth on a heater surface in such a circumstance, under microgravity, with maximum simplicity using a combination of two 1D spherical models. In one case, knowing the initial non-uniform temperature distribution given by measurement and computation at the moment of nucleation, the highest temperature, the local heater surface temperature, is taken as a uniform temperature to compute the bubble growth. This is illustrated in Fig. 4(b), and is referred to as the initial uniform superheat model, discussed in detail in Lee and Merte [10]. This model is regarded as the upper bound to the bubble growth rate possible since the highest temperature is presumed to exist uniformly throughout the liquid. The other model for the bubble growth is obtained by considering that the initial non-uniform spherically symmetric temperature distribution around the bubble is identical to that normal to the heater surface at the moment of nucleation, illustrated in Fig. 4(c). This is the minimum temperature distribution in the radial direction in realistic temperature fields surrounding the initial vapor bubble, and is regarded as the lower bound to the bubble growth rate. When comparing the presumed thermal boundary layer around the vapor bubble in Fig. 4(a) to that in Fig. 1, it becomes obvious that reality should exist between the upper and lower bounds of these temperature distributions.

The governing equations and numerical schemes for the initial non-uniform temperature distribution model are identical to those of Lee and Merte [10], except for the initial condition. A step constant and uniform heat flux input to the gold film heater described above corresponds, in microgravity, reasonably well to the transient heat conduction in a semi-infinite solid, with the temperature distribution in the liquid at the nucleation time t^* given by:

$$T(r,t^*)-T_0=\frac{2q_l''\sqrt{(\alpha t^*/\pi)}}{k_l}\exp\left(\frac{-r^2}{4\alpha t^*}\right)-\frac{q_l''r}{k_l}\operatorname{erfc}\left(\frac{r}{2\sqrt{(\alpha t^*)}}\right). \quad (1)$$

4. RESULTS AND DISCUSSIONS

Bubble growth is a result of the liquid superheat temperature distribution at the moment of nucleation,

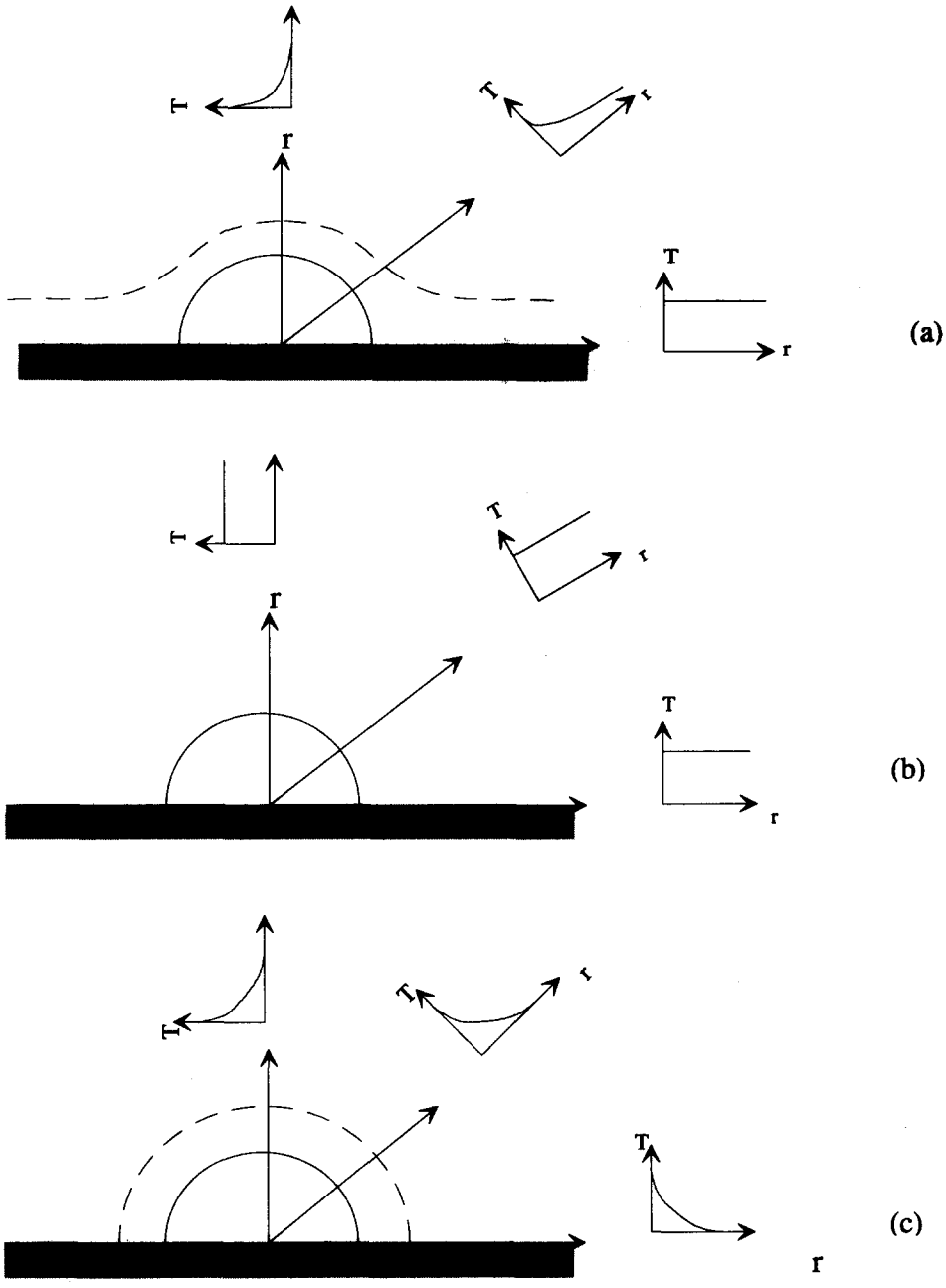

Fig. 4. Schematic diagram of hemispherical vapor bubble growing on a flat heater surface into an initially non-uniform one-dimensional Cartesian temperature. (a) Realistic thermal boundary layer, (b) initial uniform superheat model, (c) initial non-uniform superheat model.

whether resulting from heterogeneous or homogeneous nucleation. However, based on present observations, the level of superheat will be quite different between these, with what appears to be homogeneous nucleation producing the rough interface and violent bubble growth rates referred to above. Such behaviors are not considered here.

4.1. *Photographs of bubble growth*

A typical photograph taken during early vapor bubble growth is shown in Fig. 5, where the upper half presents the side view and the lower half is the bottom view through the semi-transparent gold film heater. The bright spots in the lower left are the binary time indicators. The thermistors and support tubes can be seen in the center of each heater in the bottom view, to measure the liquid temperatures above the heater surface at 1, 5 and 10 mm. A bubble in the side view appears to be hemispherical, along with its reflection from the heater surface. The same bubble also appears on the heater surface through the bottom view, giving a virtual image of two thermistor support tubes. It is

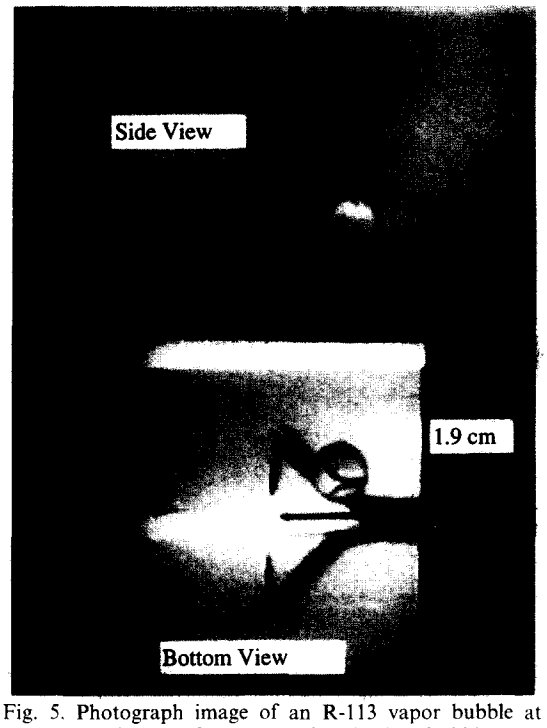

Fig. 5. Photograph image of an R-113 vapor bubble at approximately 0.01 s from onset of nucleation. Bubble number s60r9, a/g = 10^{-4}, $t^* = 30.52$ s, $q''_T = 1.8$ W cm^{-2}, $P_{sys} = 107.7$ kPa, $T_{sat} = 49.4$°C, $T_{bulk} = 48.6$°C, $T^*_w = 93.7$°C, $\Delta T_{sup} = 64$°C, $\Delta T_{sub} = 0.7$°C.

noted that the bubble shape is quite spherical and the sharp image of the tubes indicates that the interface of the bubble is smooth. The bubble size of approximately 8.3 mm diameter was determined by using imaging software, in which the projected area of the bubble was scanned, and the effective radius determined. The first bubble appeared at 30.52 s following the application of the imposed heat flux of 1.8 W cm^{-2}, defined as the nucleation delay time (t^*).

For purposes of comparing the measured vapor bubble growth with computations from the present model, two typical sets of measurements out of the 27 runs conducted in the three space experiments were selected and are presented below. The remainder of the results are available in Merte *et al.* [12]. One image was already shown in Fig. 5, corresponding to bubble number s60r9, and the other sequence of photographs is shown in Fig. 6, corresponding to bubble number s60r4. Only one image was available with a smooth interface in the former case since the maximum camera speed of 100 fps was not sufficient to capture the motion, while in the latter case the motion was slow enough to be recorded at this camera speed. The series of photographs in Fig. 6 shows every other frame, with the first bubble appearing following a nucleation delay time (t^*) of 0.74 s. The times under each photograph begin from the onset of growth. Once the frontal interface deforms as shown at $t = 0.38$ s, the measurements of bubble sizes were discontinued.

The bubble growth measurements from Figs. 5 and 6 are plotted in Figs. 7 and 8, respectively, with the computational results of the upper and lower bound models; the upper bound of the growth is computed using the initial uniform superheat model associated with the highest temperature at the heater surface, while the lower bound is computed using the initial non-uniform superheat model. In addition, the initial liquid superheat temperature distribution is superimposed as shown. The initial liquid temperature distribution was generated using the 1D analytical transient conduction analysis with the aid of the measurements of the mean heater surface temperature and a 3D transient heat conduction computation with composite materials of R-113 and the thin gold film on a quartz substrate, to determine the local heater surface temperature at each nucleation site.

4.2. *Bubble growth fraction*

The concept of a bubble growth fraction (F_{BG}) is introduced here to describe the actual vapor bubble growth in terms of a combination of the upper and lower bound curves in Figs. 7 and 8. If R_U is the radius at a time t corresponding to a point (U) on the upper bound curve, as seen in Fig. 7, and R_N is the radius at the same time corresponding to a point (N) on the lower bound curve, and R_A is the radius of an actual bubble at a point (A), a simple relationship is established as:

$$R_U \times F_{BG} + R_N(1 - F_{BG}) = R_A \tag{2}$$

Solving for F_{BG}:

$$F_{BG} = \frac{R_A - R_N}{R_U - R_N} \tag{3}$$

Using equation (3) F_{BG} is evaluated as 0.73 in Fig. 7, and plotted as shown. F_{BG} may be considered as an index of whether the vapor bubble growth is governed primarily by the upper bound, the lower bound, or by a mixture of these.

The thermal boundary layers at nucleation in Figs. 7 and 8 differ considerably in their thickness, being approximately 3 and 0.5 mm, respectively. The larger value of 3 mm is ascribed to the longer delay time of $t^* = 30.52$ s albeit at a lower heat flux level of 1.8 W cm^{-2}, while the thin layer of 0.5 mm is related to the short delay time of $t^* = 0.74$ s, with a high heat flux level of 6.5 W cm^{-2}. The measurement of the single bubble radius shown in Fig. 7, corresponding to $F_{BG} = 0.73$, is a consequence of the larger thermal boundary layer, which promotes the larger bubble growth rate and thus is closer to the initial uniform superheat model. This is contrasted with Fig. 8, in which the thinner boundary layer produces bubble growth behavior closer to the initial non-uniform superheat model, with $F_{BG} = 0.16$.

It is to be noted that the lower bound curve in Fig. 8, the initial non-uniform superheat model, is representative of the radial temperature distribution at the top of a hemispherical bubble as the bubble

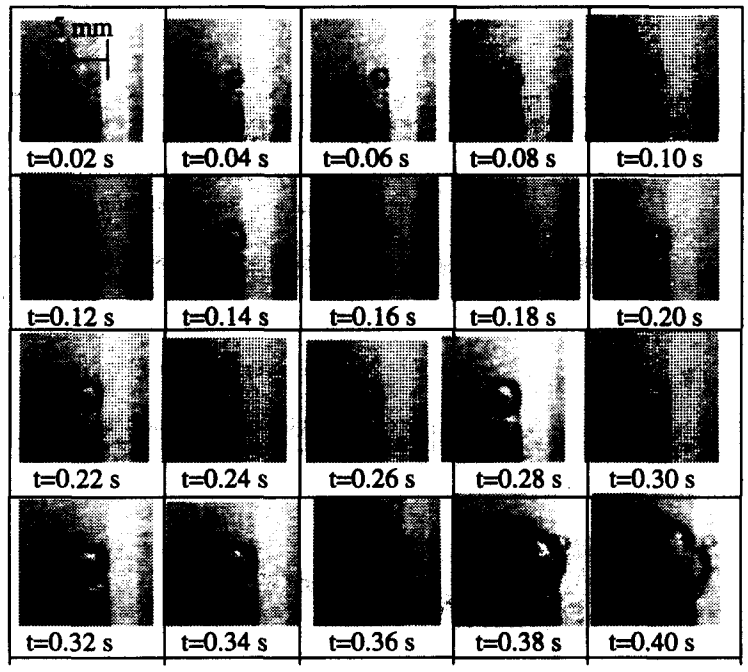

Fig. 6. Series of photographs. Bubble number s60r4, R-113, a/g = 10^{-4}, t^* = 0.74 s, q''_T = 6.5 W cm^{-2}, P_{sys} = 117.3 kPa, T_{sat} = 52.0°C, T_{bulk} = 48.8°C, T^*_w = 86.3°C, ΔT_{sup} = 20°C, ΔT_{sub} = 3.2°C.

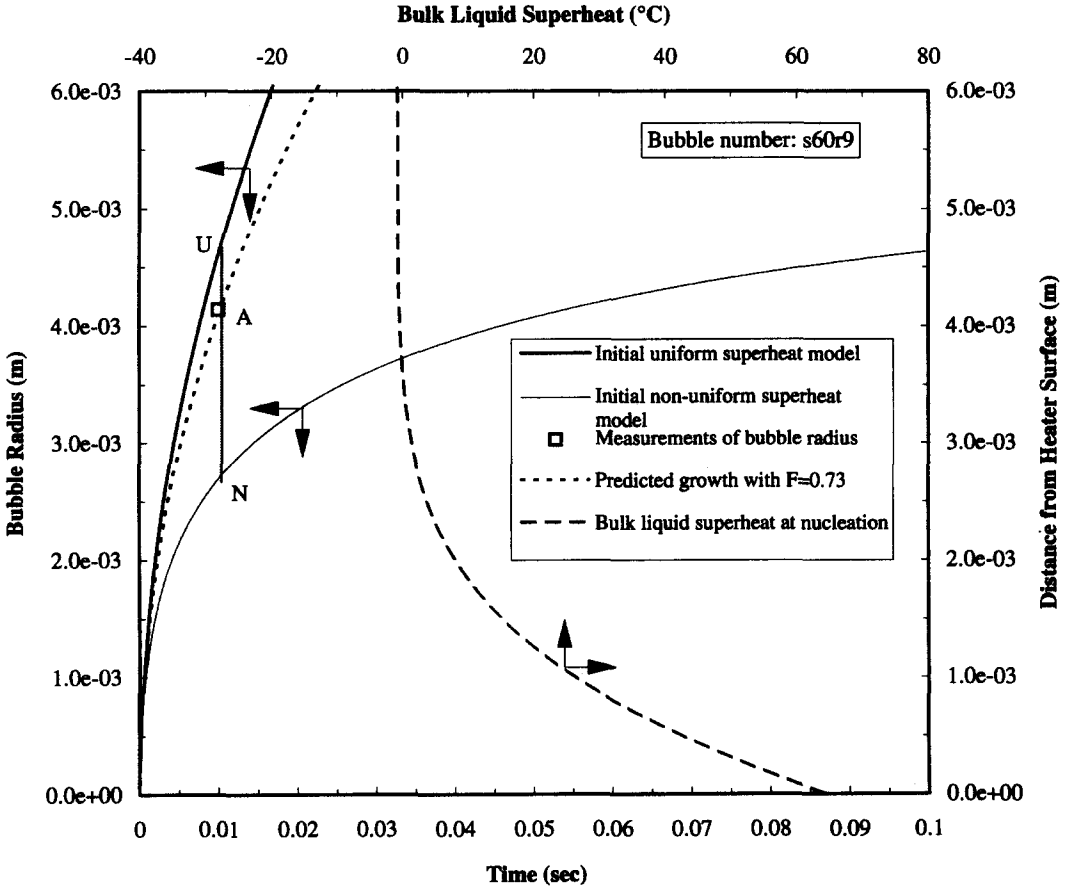

Fig. 7. Comparison of bubble growth measurements with several models. Bubble number s60r9 : a/g = 10^{-4}, t^* = 30.52 s, q''_T = 1.8 W cm^{-2}, P_{sys} = 107.7 kPa, T_{sat} = 49.4°C, T_{bulk} = 48.6°C, T^*_w = 93.7°C, ΔT_{sup} = 64°C, ΔT_{sub} = 0.7°C.

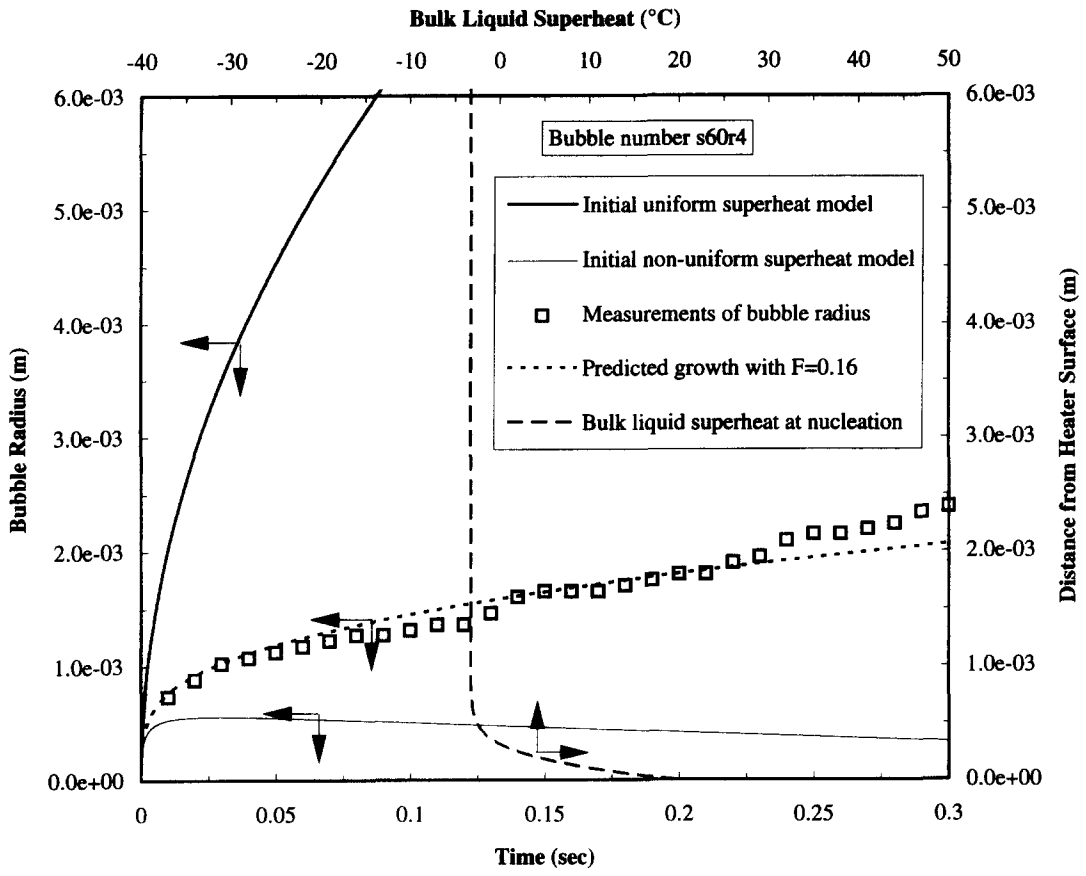

Fig. 8. Comparison of bubble growth measurements with several models. Bubble number s60r4 : a/g = 10^{-4}, $t^* = 0.74$ s, $q''_T = 6.5$ W cm^{-2}, $P_{sys} = 117.3$ kPa, $T_{sat} = 52.0$°C, $T_{bulk} = 48.8$°C, $T^*_w = 86.3$°C, $\Delta T_{sup} = 20$°C, $\Delta T_{sub} = 3.2$°C.

growth takes place. Therefore, the slight decrease of the lower bound curve in Fig. 8 is attributed to the condensation taking place at the top of the bubble. It is recognized that while the hemispherical model here incorporates the condensation at the bubble cap in cases where the bulk liquid is subcooled, the effects of microlayer evaporation beneath the vapor bubble are not included. Nevertheless, the model appears to provide, on a global basis, a reasonable description of bubble growth in microgravity. A treatment of the roles of the microlayer and the heater surface substrate in vapor bubble dynamics is given by Mei *et al.* [13].

4.3. *Bubble dynamics*

Several interesting aspects of the dynamics associated with vapor bubble growth were disclosed in the course of computing the vapor bubble growths for the two limits of initial uniform and non-uniform liquid superheats in Figs. 7 and 8. The elements of bubble radius and velocity, acceleration, and superheat at the liquid–vapor interface arising from the computations are plotted in Figs. 9 and 10 for the conditions of Figs. 7 and 8, respectively, and the differences in behavior arising from the respective initial temperature distributions will be examined. A logarithmic time scale is used in order to make more clear the events taking place in the early stages of growth.

It is seen in Fig. 9(c) that the initial critical size vapor bubble, in which the higher vapor pressure corresponding to the bulk temperature mechanically balances the surface tension, appears to sustain its critical size at a constant value for a certain period of time. In actuality it is growing, although very slowly with a velocity of 1×10^{-5} m s^{-1}, too small to be detected in this plot. The growth then suddenly increases to a velocity of approximately 13.5 m s^{-1}, due to the rapid reduction in the surface tension. This behavior is to be contrasted with that in Fig. 10(b), for the relatively low initial heater surface superheat of 20°C, in which the maximum velocity reaches only 6 m s^{-1}. The critical size bubble of 4×10^{-8} m radius in Fig. 9(c), which is beyond a measurable size, accelerates to a maximum value of 7×10^{8} m s^{-2} in Fig. 9(a), imparting momentum to the liquid, which then leads to an overshoot, resulting in a rapid decrease in liquid–vapor interface temperature, Fig. 9(b). This overshoot produces a small dip in the radius curve at approximately 1×10^{-5} s. The dip could not be detected in the plot of Fig. 7 because of its short duration, and also does not appear in the case with the thin thermal boundary layer in

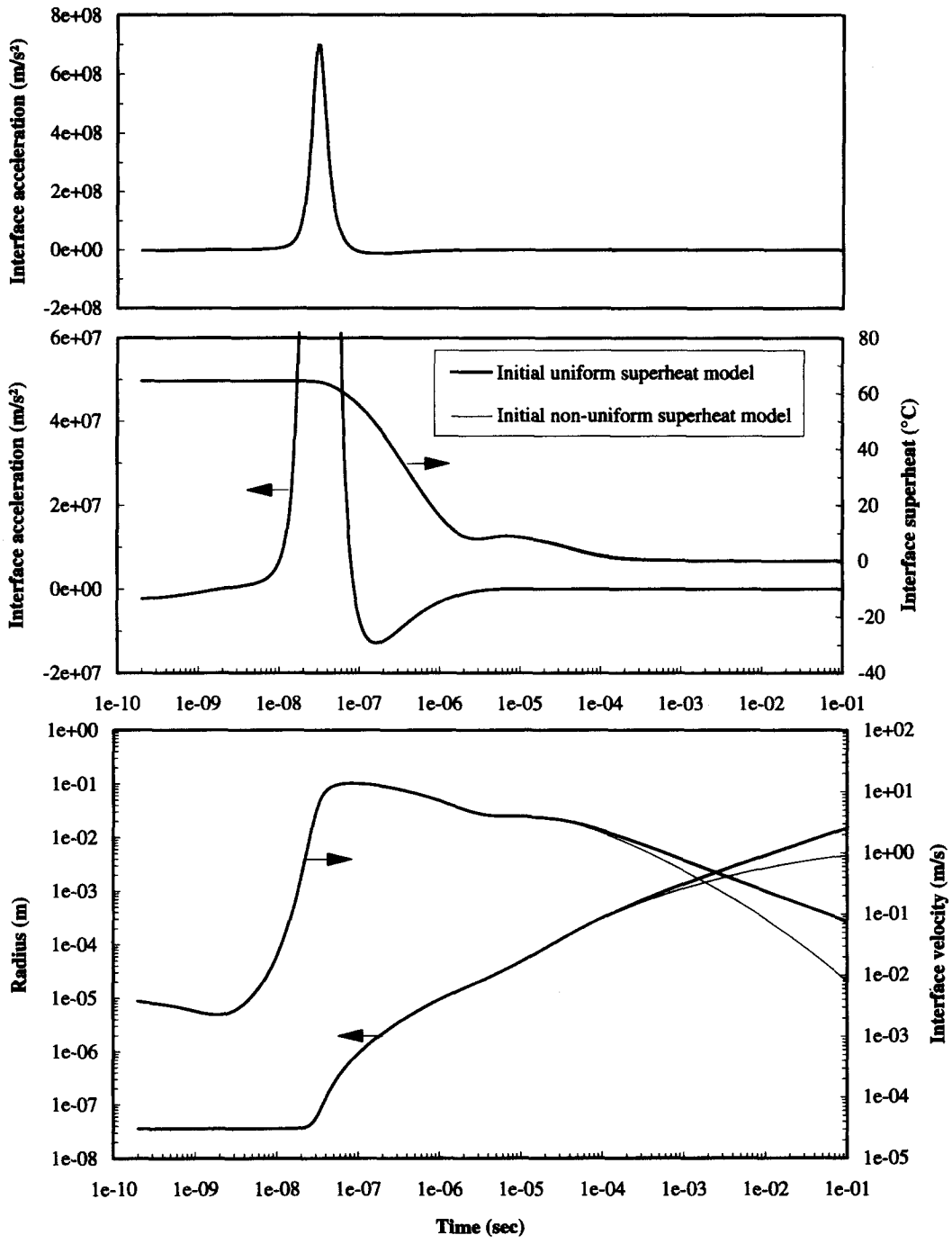

Fig. 9. Computed dynamics of vapor bubble growth model limits for bubble number s60r9 in Figs. 5 and 7. (a) Acceleration, (b) interface superheat and acceleration, (c) bubble radius and interface velocity. $\Delta T_{sup} = 64°C$.

Fig. 10(b). This would indicate that the momentum imparted to the liquid is insufficient to produce such a dip here.

In examining both Figs. 9(b) and 10(a), it is noted that no significant difference exists between the initial uniform superheat model and the initial non-uniform superheat model with respect to both the interface accelerations and the interface temperatures. The radius and velocity curves generated by both models coincide up to 1×10^{-4} s in Fig. 9(c) and up to 1×10^{-5} s in Fig. 10(b), which leads to the conclusion that the differences between the initially uniform and non-uniform liquid superheats have no effects on the early stages of bubble growth as long as the initial heater

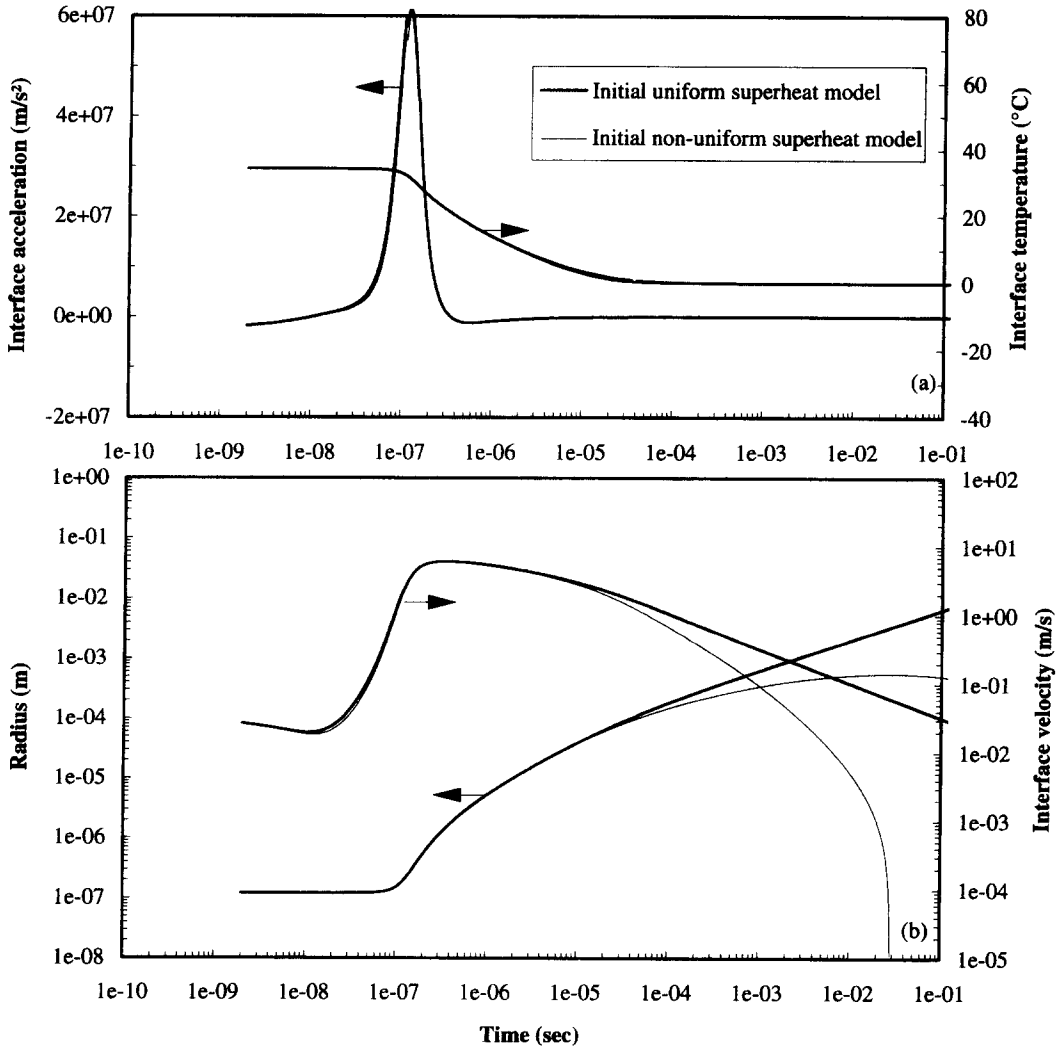

Fig. 10. Computed dynamics of vapor bubble growth model limits for bubble number s60r4 in Figs. 6 and 8. (a) Interface superheat and acceleration, (b) bubble radius and interface velocity. $\Delta T_{sup} = 20°C$.

surface superheat is common to both. It is only in the latter stages of growth that significant differences arise, as demonstrated in Figs. 7 and 8.

4.4. *Bubble boundary layer temperature distribution*

The temperature distribution in the thermal boundary layer surrounding a growing (or collapsing) vapor bubble changes as a consequence of evaporation (or condensation), diffusion to the bulk liquid and convection effects associated with the bubble growth (or collapse). To examine this behavior the computed transient temperature distributions for the two cases with high and low initial heater surface superheats described above are plotted in Figs. 11 and 12, respectively, for the initially non-uniform liquid superheats. The spatial coordinate is referenced to the continuously moving liquid–vapor interface of the vapor bubble.

Logarithmic scales are adopted in Figs. 11(b) and 12(b) in order to show the detailed behavior in the vicinity of the liquid–vapor interface. It is observed in Figs. 11(a) and 12(a) that as the bubble growth takes place the effect of the liquid divergence is to substantially increase the temperature gradient toward the bulk liquid, while the temperature gradient toward the liquid–vapor interface decreases as a result of the evaporation. These serve to rapidly diminish the non-uniform superheat initially surrounding the bubble. The initial thermal boundary layers of 3 mm and 0.6 mm in thickness in Figs. 11(a) and 12(a) are dissipated in about 0.06 s and 0.004 s, respectively. It is noted that the temperature gradient changes sign at time t8 in Fig. 12 (a), resulting in condensation at the interface. This phenomena is also observed in the latter stages in Fig. 10(b).

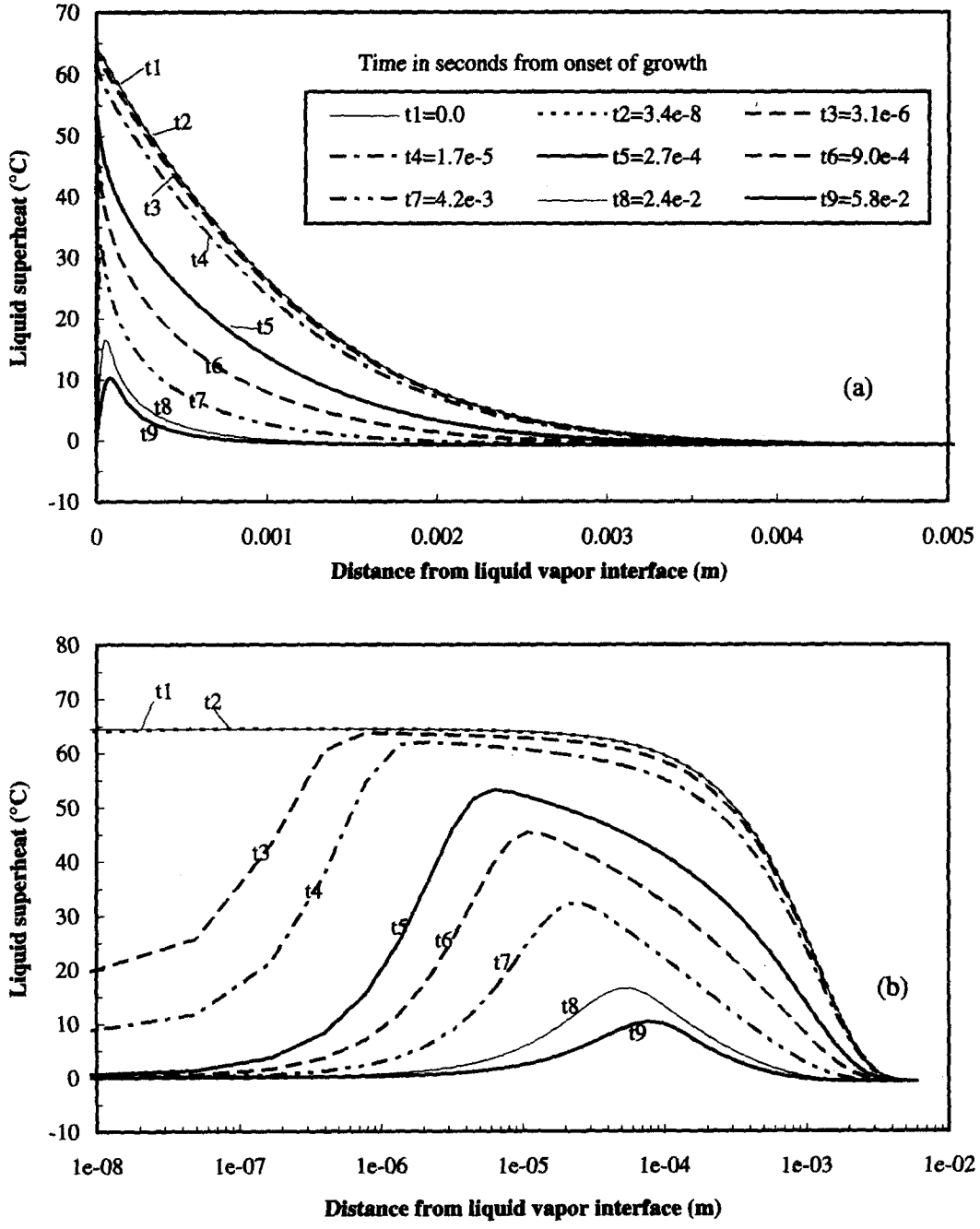

Fig. 11. Transient liquid temperature distribution for bubble number s60r9 computed by the initial non-uniform superheat model. (a) Linear scale, (b) logarithmic scale. $\Delta T_{sup} = 64°C$.

5. CONCLUSIONS

The measurements of vapor bubble growth on a flat heater surface under microgravity were compared to hemispherical models, consisting of a combination of an initially uniform and a non-uniform superheated liquid model. These models globally describe the vapor bubble growth under microgravity and determine the upper and lower bounds of the growth. Bubble growth fractions deduced from the upper and lower bounds provide a useful index to describe the growth, indicating the relative contributions between these bounds. The bubble growth rate depends upon the initial temperature distribution around the bubble, which is directly related to the heat flux and heating time leading to nucleation. The very early stages of the bubble growth are shown to be virtually the same for the initially uniform and non-uniform liquid

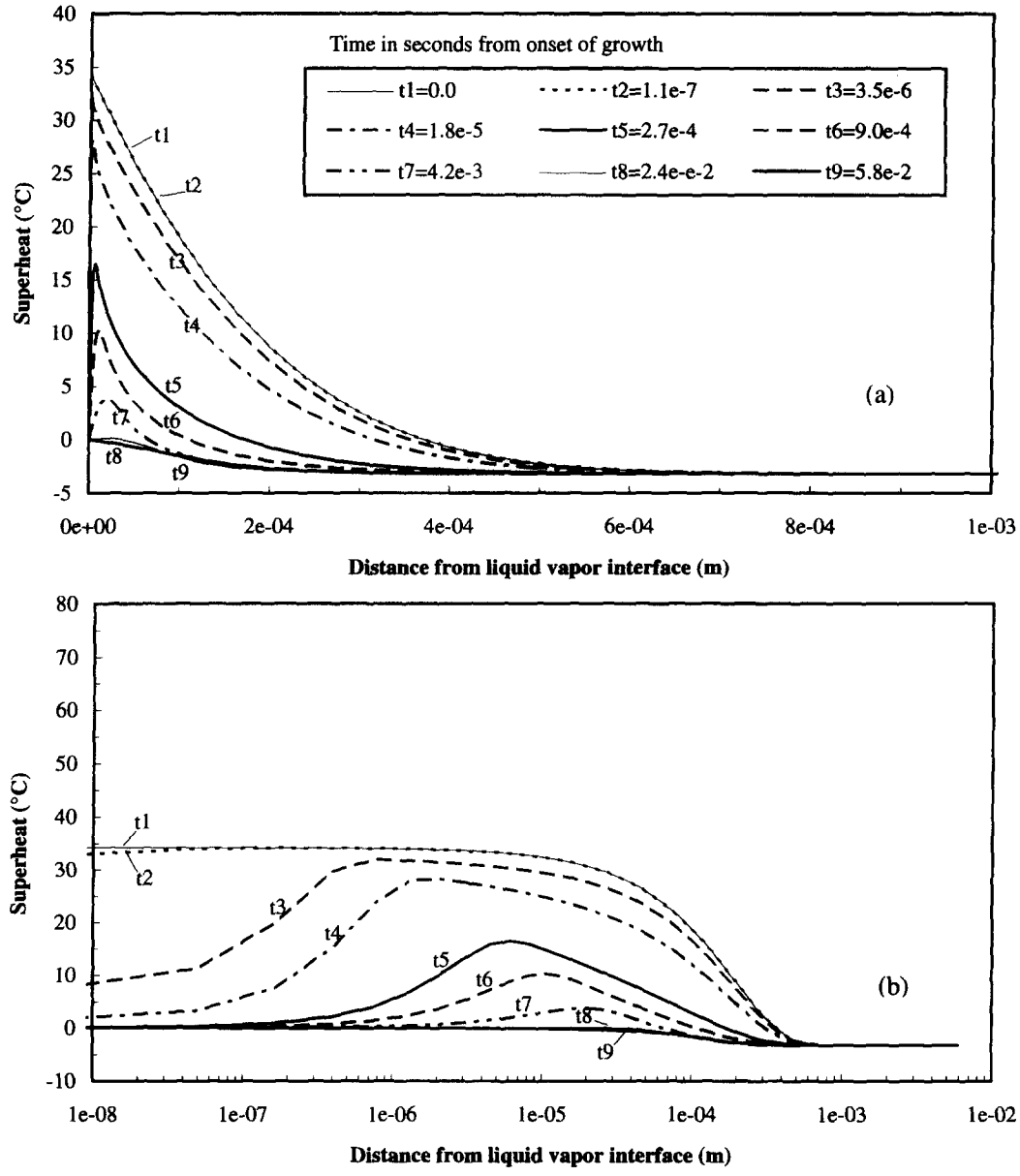

Fig. 12. Transient liquid temperature distribution for bubble number s60r4 computed by the initial non-uniform superheat model. (a) Linear scale, (b) logarithmic scale. $\Delta T_{sup} = 20°C$.

superheat cases. The transient temperature distribution surrounding a growing vapor bubble is affected substantially by the liquid divergence as well as by the transient heat conduction to the liquid–vapor interface of the bubble as a result of evaporation.

Acknowledgements—This work was conducted under NASA Contract NAS 3-25812. The interest and support of Dr Fran Chiaramonte and Mr Jack Salzman of the NASA Lewis Research Center are gratefully acknowledged. The authors give particular thanks to the team headed by Mr Dave Francisco and Mr Angel Otero for the virtually flawless performance of the equipment.

REFERENCES

1. C. M. Usiskin and R. Siegel, An experimental study of boiling in reduced and zero gravity fields. *J. Heat Transfer* **83**(3), 243–253 (1961).
2. H. Merte, Jr and J. A. Clark, Boiling heat transfer with cryogenic fluid at standard, fractional, and near-zero gravity, *J. Heat Transfer* **86C**, 315–319 (1964).
3. J. W. Littles and H. A. Walls, Nucleate pool boiling of Freon 113 at reduced gravity levels, *Proceedings of the Fluid Engineering Heat Transfer and Lubrication Conference*, 70-HT-17 (1970).
4. J. S. Ervin, H. Merte, Jr, R. B. Keller and K. Kirk, Transient pool boiling in microgravity, *Int. J. Heat Mass Transfer* **35**(3), 659–674 (1992).
5. J. Straub, J. Winter, G. Picker, H. Merte, Jr and A. Kono, Study of vapor bubble growth in a supersaturated

liquid, 8th European Symposium on Materials and Fluid Science in Microgravity, Brussels, Belgium, 12–16 April (1992).
6. H. Merte, Jr, H. S. Lee and J. S. Ervin, Transient nucleate pool boiling in microgravity—Some initial results, *Microgravity Sci. Technol.* **7**(2) 173–179 (1994).
7. Y. Abe, T. Oka, Y. H. Mori and A. Nagashima, Pool boiling of a non-azeotropic binary mixture under microgravity, *Int. J. Heat Mass Transfer* **37**(16), 2405–2413 (1994).
8. C. Y. Han and P. Griffith, The mechanism of heat transfer in nucleate pool boiling—I, *Int. J. Heat Mass Transfer* **8**, 887–904 (1965).
9. B. B. Mikic, W. M. Rohsenow and P. Griffith, On bubble growth rate, *Int. J. Heat Mass Transfer* **13**, 657–666 (1970).
10. H. S. Lee and H. Merte, Jr, Spherical vapor bubble growth in uniformly superheated liquids, *Int. J. Heat Mass Transfer* **39**, 2427–2449 (1996).
11. J. Straub, M. Zell and B. Vogel, Personal communication (December 1992).
12. H. Merte, Jr, H. S. Lee and R. B. Keller, Report on pool boiling experiment flown on STS-47-57-60, Report No. UM-MEAM-95-01, Department of Mechanical Engineering and Applied Mechanics, The University of Michigan, Ann Arbor, Michigan, NASA Contract NAS 3-25812 (1995).
13. R. Mei, W. Chen and J. F. Klausner, Vapor bubble growth in heterogeneous boiling—I. Formulation, *Int. J. Heat Mass Transfer* **38**, 909–919 (1995).